

The Dynamics of Three-Planet Systems: an Approach from Dynamical System

Bungo Shikita¹, Hiroko Koyama^{2,3}, & Shoichi Yamada^{1,3}

shikita@heap.phys.waseda.ac.jp

Received _____; accepted _____

¹Science and Engineering, Waseda University, 3-4-1 Okubo, Shinjuku, Tokyo 169-8555, Japan

²Department of Physics, Nagoya University, Nagoya, 464-8602, Japan

³Advanced Research Institute for Science and Engineering, Waseda University, 3-4-1 Okubo, Shinjuku, Tokyo 169-8555, Japan

ABSTRACT

We study in detail the motions of three planets interacting with each other under the influence of a central star. It is known that the system with more than two planets becomes unstable after remaining quasi-stable for long times, leading to highly eccentric orbital motions or ejections of some of the planets. In this paper, we are concerned with the underlying physics for this quasi-stability as well as the subsequent instability and advocate the so-called "stagnant motion" in the phase space, which has been explored in the field of dynamical system. We employ the Lyapunov exponent, the power spectra of orbital elements and the distribution of the durations of quasi-stable motions to analyze the phase space structure of the three-planet system, the simplest and hopefully representative one that shows the instability. We find from the Lyapunov exponent that the system is almost non-chaotic in the initial quasi-stable state whereas it becomes intermittently chaotic thereafter. The non-chaotic motions produce the horizontal dense band in the action-angle plot whereas the voids correspond to the chaotic motions. We obtain power laws for the power spectra of orbital eccentricities. Power-law distributions are also found for the durations of quasi-stable states. All these results combined together, we may reach the following picture: the phase space consists of the so-called KAM tori surrounded by satellite tori and imbedded in the chaotic sea. The satellite tori have a self-similar distribution and are responsible for the scale-free power-law distributions of the duration times. The system is trapped around one of the KAM torus and the satellites for a long time (the stagnant motion) and moves to another KAM torus with its own satellites from time to time, corresponding to the intermittent chaotic behaviors.

Subject headings: celestial mechanics — planetary systems — solar system: general

1. Introduction

More than 300 exoplanets have been discovered so far ¹ and, interestingly, some of them have a quite different appearance from that of our solar system. The existence of so-called "eccentric planets", that is, planets with high orbital eccentricities, for example, attracts attentions of many researchers (Butler et al. 2006). Stimulated by these observations, the planetary formation theory including the origin of the eccentric planets has made substantial progress over the years (Kokubo et al. 2006). In the standard theory, terrestrial planets are thought to be formed through giant impacts of proto-planets (planets with sub-Earth masses) in crossing orbits (Chambers & Wetherill 1998). Since N-body simulations suggest that proto-planets are formed in nearly circular orbits separated by several Hill radii (Kokubo & Ida 1995), some destabilizing processes are expected to operate and make proto-planets originally in the well-separated circular orbits collide with each other and grow up to terrestrial planets.

The stability of the system with two planets around a central star has been thoroughly investigated in celestial mechanics and it is known that there exists a critical orbital separation between the planets, beyond which the planets never experience close encounters and the system remains stable forever (Marchal & Bozis 1980; Gladman 1993). The situation changes drastically, however, if another planet is added to the system. Using numerical simulations, Chambers et al. (1996) demonstrated that the systems with more than two planets become unstable even for large orbital separations. Although the planetary motions remain regular for some time at first, one of the planets eventually comes close enough to another (that is, within the Hill radius of the latter), leading to subsequent orbital crossings.

¹<http://exoplanet.eu> for the latest information.

This is a good news for the terrestrial formation theory and may also account for the formation of the eccentric planets. In fact, Marzari & Weidenschilling (2002) numerically integrated the motions of three Jupiter-mass planets and found in most of their simulations that one of the planets is ejected from the system and the others are left in the system with high eccentricities. Several attempts (Juric & Tremaine 2007; Ford & Rasio 2007) have been made to reproduce the observed eccentricity distribution by the orbital instability. Their results seem to be consistent with the observations although the latter itself may be somewhat biased (Shen & Turner 2008).

The planetary motions in these systems are interesting in their own right. As mentioned above, we commonly observe a long period of quasi-regular motions that look like independent Keplerian motions before the eventual orbital crossings. The switch is sudden and quick. The duration of the quasi-regular motions is sensitive to the initial orbital separations and eccentricities (Chambers et al. 1996; Yoshinaga et al. 1999). Using numerical simulations and simplified analytical models, Zhou et al. (2007) claimed that the gradual deviation from the Keplerian motions can be regarded as a random walk process. These efforts notwithstanding, the underlying physics behind the phenomena such as the long period of quasi-regular motions followed by the sudden transition to chaotic states is remaining to be revealed and is the main concern of this paper.

We attempt to understand this phenomenon as the so-called “stagnant motion” in the phase space, which will be described below. We pay attention to a similar phenomenon known in the field of dynamical system. In nearly integrable systems, a sudden transition from a regular motion sustained for a long time to chaotic motions is often observed. In the nonlinear lattice problems, for example, Hirooka & Saito (1968) found that an initially imposed normal mode experiences sudden energy exchanges among several other modes after long regular oscillations. They called this “the induction phenomenon” and referred

to the duration of the regular motion as "the induction period" (Saito et al. 1970).

Aizawa et al. (1989) constructed a so-called "stagnant motion" model for this induction phenomenon. According to the KAM theorem (Kolmogorov 1979; Moser 1958; Arnol'd 1963), the phase space of a nearly integrable system retains tori, which exist in the integrable system, if perturbations to the integrable system are sufficiently weak. It is generally expected that the so-called KAM tori will survive even for not so small perturbations. In the stagnant motion model, it is assumed that the KAM torus exists in "the chaotic sea", the region corresponding to chaotic motions of the system, being surrounded by a thin layer called "the stagnant layer", in which smaller tori are distributed in a self-similar manner (see Fig. 1). The system shows nearly regular behavior when the phase space orbit is trapped in the stagnant layer whereas the sudden transition to chaotic motions occur when the orbit escapes out of the layer. This model is successful in reproducing the scale-free power spectra and the distribution of the induction period. In this paper we show some evidence to support the interpretation of the motions of three-planet system as one of the induction phenomena and attempt to understand them in the frame work of the stagnant motion model.

The organization of the paper is as follows. We summarize the numerical models in section 2. In section 3, we describe the methods of analysis. The results are presented in section 4 and the summary and discussions are given in section 5.

2. Models

In this paper, we restrict the investigation to *the simplest* multi-planet system, which shows the behavior mentioned above: the system consists of a central star with $M_* = 1M_\odot$ and three planets with an identical mass in coplanar orbits. We consider two cases for the

planetary mass, m_{pl} : (1) $m_{pl} = 10^{-7}M_{\odot}$ (the proto-planet system) and (2) $m_{pl} = 10^{-3}M_{\odot}$ (the Jupiter system). The initial semi-major axis of the innermost planet is set to be $a_1 = 1\text{AU}$ for the proto-planet system and $a_1 = 5\text{AU}$ for the Jupiter system. Following Chambers et al. (1996), we give the initial radial locations of the outer planets as

$$a_{i+1} = a_i + \Delta r_{h(i,i+1)}, \quad (1)$$

where a_i is the semi-major axis of the i -th planet counted from the innermost one, and $r_{h(i,i+1)}$ is the Hill radius for the pair of i -th and $i + 1$ -th planets defined as

$$r_{h(i,j)} = \left(\frac{m_i + m_j}{3M_*} \right)^{1/3} \frac{a_i + a_j}{2}. \quad (2)$$

In addition, we also consider the case with $m_{pl} = 10^{-3}M_{\odot}$, $a_1 = 5\text{AU}$, $a_2 = 7.25\text{AU}$, $a_3 = 9.5\text{AU}$, that is, the same parameter set as that used in Marzari & Weidenschilling (2002) except for no inclination in our model.

The Hamiltonian in the barycentric coordinates consists of three parts and is given as

$$\begin{aligned} H &= H_{Kep} + H_* + H_{int}, \\ H_{Kep} &= \sum_{i=1}^n \left(\frac{\mathbf{p}_i^2}{2m_i} - \frac{Gm_0m_i}{r_i} \right), \\ H_* &= \frac{\mathbf{p}_0^2}{2m_0} - \sum_{i=1}^n \left(\frac{Gm_0m_i}{r_{i0}} - \frac{Gm_0m_i}{r_i} \right), \\ H_{int} &= - \sum_{\substack{i,j=1 \\ i \neq j}}^n \left(\frac{Gm_im_j}{r_{ij}} \right). \end{aligned} \quad (3)$$

In the above equations, G is the gravitational constant and m_i , \mathbf{p}_i , r_i denote the mass, momentum and radial position of the i -th object, where $i = 0$ corresponds to the central star. r_{ij} stands for the distance between the i -th and j -th objects. H_{Kep} is an integrable Hamiltonian corresponding to independent Keplerian motions of three planets with respect to the barycenter. H_* is a correction originated from the orbital motion of the central star itself by the attraction of the planets. H_{int} expresses the interactions between the planets.

For each model listed in Table 1, we generate 10000 different initial conditions, which have the same integrals of motion, that is, the linear and angular momenta and total energy. This constraint is important to explore the structure in the phase space. The orbital phases of planets are given randomly. Since the radial location of the innermost planet, a_1 , is fixed, the remaining parameters, the radial locations of the outer planets, a_2 , a_3 , and the velocity of the central star, V_{sx} , V_{sy} , are determined so that the system should have the same values of the integrals of motion. As a result of this constraint, the resultant initial radial locations of the planets differ only slightly among 10000 realizations. The planets have slight eccentricity ($e \sim 10^{-7}$ for $m_{pl} = 10^{-7}$ and $e \sim 10^{-3}$ for $m_{pl} = 10^{-3}$) initially because of the non-zero velocity of the central star relative to the barycenter. Using the ensemble obtained in this way, we obtain various distributions and take statistics thereof. We summarize in Table 1 the input parameters (a_1 and the integrals of motion) as well as the orbital separations and eccentricities averaged over the 10000 realizations for each model.

Numerical integrations are performed with the MERCURY6 package, which was developed by Chambers (2000). For the proto-planet system, we integrate the orbital motions until the first close encounter occurs. For arbitrarily chosen three models among 10000 realizations, we continue the integration after the close encounter up to 10^7 years in order to compute the Lyapunov exponent and power spectra in the post-encounter phase. For the Jupiter system, The integration is terminated when one of the planets is ejected from the system.

Before closing this section, we discuss the relative magnitude of each part of the Hamiltonian given in Eq. (3) and the existence of KAM tori in our system. The relative magnitude of H_* to H_{Kep} is always of the order of m_{pl}/M_* and so is the ratio of H_{int} to H_{Kep} unless r_{ij}/r_{i0} becomes as small as $\sim m_{pl}/M_*$. In our models, the value of m_{pl}/M_*

is 10^{-7} for the proto-planet system or 10^{-3} for the Jupiter system and the minimum value of r_{ij}/r_{i0} , which is achieved when two planets have the same orbital phase, is $\sim (m_{pl}/M_*)^{1/3} \gg m_{pl}/M_*$. Thus, H_* and H_{int} are always small in our models.

As mentioned in Introduction, the KAM tori exist in the phase space of the nearly integrable system, whose Hamiltonian is expressed as the sum of the integrable part $H_0(I)$ and the perturbation $\epsilon H(I, \theta)$:

$$H(I, \theta) = H_0(I) + \epsilon H(I, \theta) \quad (\epsilon \ll 1), \quad (4)$$

provided the perturbation is sufficiently small. Here I and θ are the action and angle variable, respectively. It should be noted that our Hamiltonian does not meet this condition. Hence we look for evidence that this is really the case, employing the Lyapunov exponent, power spectra of orbital elements and induction periods, in addition to the trajectories in the $I - \theta$ plane, which will be described in the following section.

3. Analysis Methods

In order to get some insight into the phase space structure of our models, we employ three tools, that is, the Lyapunov exponent, the power spectra of orbital elements and the distribution of the duration of the quasi-regular motions. The first two are useful to see the degree of chaos of the system. If there remain KAM tori in the phase space indeed, the system is expected to show both non-chaotic and chaotic features, which will then be captured by these measures. The last quantity will tell us if the planetary motions of our models can be interpreted as the induction phenomenon. In fact, the distribution is expected to have a power law if it is really the case.

3.1. Lyapunov exponent

We compute the so-called maximum Lyapunov exponent. The maximum global Lyapunov exponent, λ_{global} , is the local growth rate of the distance, $\| \delta \mathbf{x}(t) \|$, between adjacent orbits in the phase space and is defined more precisely as

$$\lambda_{global} \equiv \lim_{T \rightarrow \infty} \frac{1}{T} \log \frac{\| \delta \mathbf{x}(T) \|}{\| \delta \mathbf{x}(0) \|}. \quad (5)$$

It is, of course, impossible in practice to compute the growth of the distance over the infinite time. We calculate instead the following quantity as a function of time and look into their behavior:

$$\lambda_{global}(t) = \frac{1}{t} \log \frac{\| \delta \mathbf{x}(t) \|}{\| \delta \mathbf{x}(0) \|}. \quad (6)$$

The asymptotic limit of this function at $t \rightarrow \infty$ gives the original Lyapunov exponent.

The integrable system has a null Lyapunov exponent while chaotic systems have a positive Lyapunov exponent. If the system is nearly integrable in particular, the Lyapunov exponent defined by Eq. (6) oscillates around a small but finite positive value and does not converge as $t \rightarrow \infty$.

In analyzing the system that shows both quasi-regular and chaotic behaviors alternatively, it is useful to look also into the local Lyapunov exponent, λ_{local} , which is the same local growth rate of the orbital separation in much shorter times and is expressed as

$$\lambda_{local}(n, \tau) \equiv \frac{1}{\tau} \log \frac{\| \delta \mathbf{x}(n\tau) \|}{\| \delta \mathbf{x}((n-1)\tau) \|}, \quad (7)$$

where n specifies an interval with a period of τ . The choice of τ is rather arbitrary. It should be longer than the typical orbital period but shorter than the time scale of the quasi-regular or chaotic motions of interest. If chosen appropriately, it will indicate the local degree of chaos.

In the following, the interval, τ , for the local Lyapunov exponent is chosen to be 100 years, which corresponds to $10 \sim 100$ times the orbital periods. Both λ_{global} and λ_{local} are

obtained by numerically integrating the linearized equations of motion along the phase space orbit given by the integration of the equations of motion (Wolf et al. 1985).

3.2. Power spectra of orbital elements

The power spectrum, $S(f)$, of an orbital element denoted by $z(t)$ is defined as

$$S(f) \equiv \left| \int_0^\infty z(t) e^{ift/2\pi} dt \right|^2 \quad (8)$$

and is also useful to characterize the chaotic system. If one defines the autocorrelation function of $z(t)$ as

$$\Phi_z(\tau) \equiv \lim_{T \rightarrow \infty} \frac{1}{2T} \int_{-T}^T z(t) z(t + \tau) dt, \quad (9)$$

its Fourier transform is equal to the power spectrum according to the Wiener-Khinchin theorem (e.g. Leichl 1980):

$$S(f) = \int_{-\infty}^\infty \Phi_z(\tau) e^{-if\tau/2\pi} d\tau. \quad (10)$$

Hence by investigating the power spectrum, we can acquire the knowledge of the temporal autocorrelation of the orbital element.

The integrable systems have a discrete spectrum with peaks at the orbital periods provided appropriate variables are chosen. On the other hand, the chaotic systems have a rather featureless continuum spectrum. In particular, it is known that the nearly integrable systems show in general a power-law spectrum in their low frequency regime as

$$S(f) \propto f^{-\nu} \quad (11)$$

indicating a long-time correlation for the variables.

In this paper, we discuss the power spectra of the orbital eccentricity, e_i , for each planet in the system. We confirmed, however, that other orbital elements such as the semi-major axis give a similar result.

3.3. Distribution of induction periods

It is known for the induction phenomena that the distribution of the induction periods, T , or the duration of quasi-regular motions generally obeys a power law,

$$P(T) \propto T^{-\beta} \quad (\beta > 0), \tag{12}$$

for large T (Baouer & Bertsch 1990). This implies that there is no characteristic time scale for the induction period. This type of distribution can be obtained in the stagnant motion model by evoking a collection of tori, which have a self-similar distribution, in the so-called stagnant layer around a KAM torus in the phase space (Aizawa et al. 1989). Fig. 1 illustrates schematically the phase space structure assumed in the stagnant motion model. The stagnant layer is filled with self-similarly distributed tori, which trap the system around them for a long time. Since the trapping time is scale free thanks to the self-similar distributions of the tori, the power law is obtained for the induction period, which is nothing but the trapping time.

We will use this feature to see if the planetary motions of our concern are indeed the induction phenomenon. We expect that the duration of quasi-regular motions corresponds to the induction period. More precisely, we define the duration of the regular motion as the interval from the start of the integration of motion until the first close encounter between two planets. The close encounter means here that the pair of planets has the distance between them smaller than their Hill radius. It is known from the previous papers and confirmed in this paper that the transition from the regular motion to the chaotic one occurs in general after the first close encounter (Chambers et al. 1996). Incidentally, since the ejection of one planet occurs rather soon after the encounter for the Jupiter system, we also study the distribution of the time from the encounter to the ejection.

4. Results

4.1. Lyapunov exponents

We first show in Fig. 2 the evolution of the orbital semi-major axis and eccentricity of each planet for model 11, which is representative of the proto-planet system. In this model, the first close encounter between two planets occurs at $t = 16400\text{yr}$. Before the encounter, the planetary motions are almost regular and the orbital elements remain unchanged essentially. After the encounter, on the other hand, they start to vary on short time scales. Then comes a period ($t \simeq 23500 - 38500\text{yr}$) when the semi-major axes do not change very much and the eccentricities for two planets vary rather monotonically in this period. Thereafter the orbital elements change in time violently again. Note, however, that the quasi-regular phases, although with much shorter periods, emerge intermittently.

In Fig. 3, both the global and local Lyapunov exponents, $\lambda_{global}(t)$ and $\lambda_{local}(n, \tau)$, are displayed as a function of time for the same model as in Fig. 2. As mentioned earlier, the time interval τ for the integration of the local Lyapunov exponent is set to be 100yr, that is roughly 100 times the orbital period for the proto-planet system, whose innermost planet is initially located at 1AU. It is clear that $\lambda_{global}(t)$ monotonically decreases toward zero before the close encounter ($\lambda \simeq 0.0005$ just prior to the encounter), indicating that the motions are non-chaotic (or very weakly chaotic) in this phase. After the encounter, on the other hand, $\lambda_{global}(t)$ increases drastically by about two orders of magnitude and fluctuates slowly around a constant value (~ 0.02) thereafter. For comparison, we also employ MEGNO, another indicator of chaos suggested by Cincotta & Simó (2000), to estimate the global Lyapunov exponent. The values derived from MEGNO agree with the ones obtained above within 1% typically.

The local Lyapunov exponent also shows that the orbital motions are almost non-

chaotic before the encounter. In fact, the almost constant small value during this period is consistent with the evolution of the global Lyapunov exponent for the first 100yr. It is also clear that the local Lyapunov exponent shows remarkable peaks rather intermittently after the close encounter. Moreover, it is found by the comparison between Figs. 2 and 3 that λ_{local} takes a small constant value when the semi-major axis of each planet remains nearly constant in time. It is interesting to point out again that the eccentricities of planetary orbits are not zero and change in time during this period. This suggests that the planetary system is settled to a quasi-stable configuration what is different from the initial condition and has substantial orbital eccentricities.

In Fig. 4, we show the orbital evolution of the Jupiter system (model 17). In this model, the first close encounter happens at $t = 162416\text{yr}$ and one of the planets is ejected from the system at $t = 239279\text{yr}$. Just as in the proto-planet system shown in Fig. 2, the semi-major axes remain almost unchanged in time and the eccentricities oscillate around the initial value with small amplitudes before the close encounter but they start to vary rapidly in time after the encounter. It is noted that the amplitudes of the variations are much larger for the Jupiter system than those for the proto-planet system, the fact responsible for the ejection of a planet in short times in the Jupiter system.

In Fig. 5, the global and local Lyapunov exponents are shown for the same Jupiter system. Again we see the monotonic decrease of the exponent for the first $\sim 20000\text{yr}$. In this case, however, the exponent is then saturated and stays at a small but finite level. This reflects the fact that the system is close to integrable but still non-integrable. The global Lyapunov exponent increases quickly after the close encounter as in the proto-planet system. The local Lyapunov exponent obtained for every 100yr, which is about 10 times the orbital period for the Jupiter system, shows some intermittent spikes after the close encounter although the interval from the close encounter to the ejection of a planet is rather

short. It is also confirmed that the violent variations of the orbital elements occur in the spikes of the local Lyapunov exponent and that when λ_{local} has a small, nearly constant value, the semi-major axes are not changed very much whereas the eccentricities are non-zero and fluctuate rather slowly. The Lyapunov exponent increases toward the ejection of the planet in this case.

The above-mentioned features in the orbital evolutions as well as in the Lyapunov exponents are common to all the models. (The behavior of the Lyapunov exponent close to the ejection of a planet is an exception and no clear trend can be seen). This suggests that the underlying structure in the phase space is not different very much from each other. In particular, the quasi-regular motions before the close encounter, which are very weakly chaotic at most, strongly suggest the existence of the KAM torus. This may be true even of the periods that occur intermittently after the close encounter, in which the local Lyapunov exponent returns to a small value and the planetary motions become quasi-regular again. Then the following picture is inferred: the phase space consists of a chaotic sea and KAM tori surrounded by a stagnant layer that consists of satellite tori. The phase space orbits go from one system of KAM torus and stagnant layer to another through the chaotic sea. When the phase space orbit is moving around one of the KAM tori, the local Lyapunov exponent takes a small constant value whereas it becomes spiky once the phase space orbit moves into the chaotic sea.

This picture is also supported by the plot in Fig. 6 of the action (I_0) and angle (θ_0) variables of the non-perturbed Hamiltonian H_{Kep} in Eq. (3). These variables are given as

$$I_{0,i} = m_i \sqrt{Gm_0 a_i}, \quad (13)$$

$$\theta_{0,i} = u_i - e_i \sin u_i. \quad (14)$$

In the above equations, the angle variable $\theta_{0,i}$ is called the mean anomaly and the so-called

eccentric anomaly, u_i , is defined as

$$\tan \frac{u_i}{2} = \sqrt{\frac{1 - e_i}{1 + e_i}} \tan \frac{\phi_i}{2}, \quad (15)$$

where e_i denotes the eccentricity and ϕ_i the orbital phase of the i -th planet measured in the barycentric coordinates. In Fig. 6, we plot the action and angle variables for the innermost planet every ten steps. The behavior of the variables for other planets is essentially the same.

One can recognize some horizontal bands and voids in the figure. These bands are regions, where the phase space orbit lingers, whereas the voids are passed through quickly. It is also seen that some of the bands undulate. The densest band pointed by an arrow at $I_{0,1} = 1.98 \times 10^{50}$ (gcm²/s) in the figure corresponds to the KAM torus of the initial regular motion and its satellite tori, whereas other bands represent other KAM tori and their satellites, which are visited by the phase space orbit during the evolution. The bands with undulation correspond to the motion approaching the ejection of a planet. Since the $I_{0,1} - \theta_{0,1}$ plane is filled by horizontal lines (or tori) everywhere uniformly if the perturbations are absent, the voids can be interpreted as chaotic regions produced by the perturbations to H_{Kep} .

Looking more closely, one finds that all the lines composing a band that corresponds to a quasi-regular motion are oscillating with finite amplitudes. These oscillations are studied by the Fourier analysis and the power spectrum for the initial quasi-regular motion is plotted in Fig. 7. It is found that the power spectrum obeys a power-law over a wide frequency range. This means that there is no characteristic frequency scale, the fact which seems to be consistent with the stagnant motion model, in which satellite tori are supposed to exist around a KAM torus with a fractal size distribution.

In the following we will further look for evidence that the dynamics in these periods, that is, a relatively long quasi-regular motions followed by an abrupt transition to chaotic

motions can be interpreted as an induction phenomenon indeed.

4.2. Power spectra of orbital eccentricities

In Fig. 8, we show the power spectra of the orbital eccentricity of the innermost planet before and after the close encounter for model 11. This is a representative model for the proto-planet system and the one we employed to demonstrate the behavior of the Lyapunov exponents in Fig. 3. This model also has a merit that it has a relatively long duration up to the first close encounter. Although the data are quite noisy, they can be roughly fit by the power law, $\propto 1/f^\nu$. It is apparent that the power-law indices are different between the two phases. We obtain $\nu = 1.01$ before the encounter whereas the spectrum becomes steeper with $\nu = 1.85$ thereafter.

The same trend can be seen also for the Jupiter system, whose typical results are displayed in Fig. 9 for model 17. Again the spectra are fit by the power law approximately both before and after the encounter and the spectral indices are $\nu = 0.88$ before the encounter and $\nu = 1.85$ thereafter. The spectrum given in the upper panel of Fig. 9 has finer features than that in the upper panel of Fig. 8 because pre-encounter phase is longer for the model in Fig. 8 than for that in Fig. 9. Note also that the post-encounter phase was computed up to the ejection of a planet in this case.

In Tables 2 and 3, we summarize the power-law spectral indices of the arbitrarily chosen three realizations for each model both before the encounter (1st phase in the table) and after the encounter (2nd phase). Although we again employ the orbital eccentricity of the innermost planet, the orbits of outer planets behave similarly. Table 2 gives the results for the proto-planet system while Table 3 corresponds to the Jupiter system. For some of the models, the duration of the phase is too short to obtain the spectral index and "-" is

put instead of the spectral index for them. Although the spectral indices vary substantially even among different realizations for the same model, it is clear that phase 2 has spectral indices clustered around $\nu = 2$ whereas phase 1 has smaller indices, $0 \lesssim \nu \lesssim 1.69$, in general. The average spectral indices over all the models in Table 2 are 0.84 and 1.84 for the phases 1 and 2, respectively. The counter parts for the Jupiter system given in Table 3 are 0.91 before the encounter and 1.77 after the encounter.

The power-law spectrum is a characteristic feature of the stagnant motions although the power-law indices are not specified by the theory. The time variations of the orbital elements are induced by the energy exchange among planets. The power-law $\propto 1/f^2$ observed for the post-encounter phase indicates that the time evolution of the orbital eccentricity is a Brownian motion with the root mean square being $\propto t^{1/2}$. On the other hand, the pre-encounter phase has a smaller spectral index in general. Although the numbers of the planets in the system are different, our results on the growth rate of eccentricity in the post-encounter phase are consistent with Zhou et al. (2007), who studied the system with 50 planets and claimed that the eccentricity of planetary orbits roughly evolves as $\langle e^2 \rangle^{1/2} \propto t^{1/2}$ both before and after the encounter. As mentioned above, however, we found for our system with three planets different power-law indices before the encounter. The smaller power-law indices of $e(t)$ in the pre-encounter phase in our models might correspond to the so-called fractional Brownian motion, for which the root mean square $\langle e^2 \rangle^{1/2}$ grows more slowly than for the ordinary Brownian motion (Mandelbrot & Van Ness 1968).

4.3. Distribution of induction periods

4.3.1. *proto-planet system*

As mentioned in section 3.3, the distributions of the durations of various phases should be one of the key ingredients if the dynamics were to be interpreted as an induction phenomenon and described by the stagnant motion model. For the proto-planet systems we study the statistics of the duration, T_{ce} , of the pre-encounter phase, where the orbits are nearly circular. We show in Fig. 10 the distribution of T_{ce} for 10000 realizations of each model for the proto-planet systems listed in Table 1. For the plots we employed 100 equal bins between the maximum and minimum values of T_{ce} . For some models with small initial orbital separations, these two values are quite different and, as a result, there are some bins with very small populations near the longest T_{ce} .

Except for the model with the smallest Δ , the distribution has a peak, which shifts to longer times as Δ becomes larger. It is also clear from the log-log plot that the dispersion around the peak gets larger, too, as Δ becomes greater. We are particularly interested in the long time regime, where the stagnant motion model predicts power laws, which implies that there is no characteristic time scale for the trapping in the stagnant layer and is supposed to be a consequence of the self-similar distribution of tori in the stagnant layer. In the figure, the straight lines are the power-law fit to the long-time part of the distributions. We employ 30 data points down from the one with the longest T_{ce} . The bins with T_{ce} shorter than that at the peak or those with the population of less than 2% are discarded. If there are less than 30 data points that satisfy the criteria, all of them are used. The obtained power-law indices lie between -5.68 to -2.27 as shown in each panel, which are expected to reflect the difference in the phase space structures.

It is obvious that the distributions are deviated from power laws both at the short

and long durations. The initial conditions prepared so that planets are initially in regular motions may lead to the underestimation of the duration time, since it might have cut short the earlier portion of the pre-encounter phase. Note, however, that there is no reason that we expect power laws for short time scales. As for the longer time scales, on the other hand, power laws are expected if the stagnant motion model can be applied. We suspect that the main reason for the deviation from the power law for the very long durations is that the number of realizations, that is 10000 for each model, are not large enough. In fact, only a small number of realizations are contributing to the longest time portion of the distributions, in which the deviation from the power law is remarkable.

In Fig. 11, we present a histogram in the $\Delta - T_{ce}$ plane expressed in color for the number of cases in our model calculations. Connecting the peak, $T_{ce,peak}$, for each Δ , we find the following relation:

$$\log T_{ce,peak} \simeq 1.008\Delta - 1.307, \quad (16)$$

which is very similar to what Chambers et al. (1996) found ($a = 1.176, b = -1.663$ in their results) with a much smaller number (5) of realizations. It is clear from our results that the relation holds only for the durations corresponding to the peaks and, in fact, the durations for each Δ have a distribution as demonstrated above. Incidentally, the integrals of motion, the linear and angular momenta and total energy, are fixed in producing different realizations in this paper, which was not the case for Chambers et al. (1996).

4.3.2. *Jupiter system*

One of the characteristics for the dynamics of the Jupiter systems is that one of the planets are ejected from the system eventually. In addition to the durations of the pre-encounter phase, T_{ce} , we take also the statistics of the time from the first close encounter until the ejection of a planet, $T_{ej} - T_{ce}$, for the Jupiter systems.

Fig. 12 shows the distributions of T_{ce} for models 17 (left panel) and 18 (right panel) for the Jupiter system. Note that model 18 is meant to mimic the models in Marzari & Weidenschilling (2002) and the initial condition is prepared differently from other models. The straight lines in the figure are the power-law fit to the long-duration part of the distributions and obtained just in the same manner as for the proto-planet systems (see Fig. 10). It is seen again that the power-law distribution is a good approximation in this regime, which suggests that the quasi-regular motions before the close encounter in the Jupiter system can be also understood as the stagnant motion just as for the proto-planet system. The obtained power-law indices are -5.57 and -1.56 for models 17 and 18, respectively.

Now we turn attention to the distributions of the time from the encounter to the ejection, $T_{ej} - T_{ce}$, which are given in Fig. 13 for models 17 (left panel) and 18 (right panel). It is clear from the figure that the long-time portions of both distributions are again approximated by the power laws with the indices of -2.65 and -2.67 for models 17 and 18, respectively. This implies that there is no characteristic time scale for the duration, during which the phase space orbit of the system remains in the part of the phase space corresponding to the bound states of three planets.

If the power-law distribution of T_{ce} reflects the self-similar distribution of smaller tori in the stagnant layer of a KAM torus (see Fig. 1) as claimed in the stagnant motion model, the power-law distribution of $T_{ej} - T_{ce}$ might suggest a self-similar distribution of these KAM tori in the part of the phase space for the bound motions of three planets (see Fig. 14 for a schematic picture of the phase space).

5. Summary and Discussions

In this paper we have numerically investigated the dynamics of the three-planet system and inferred its phase space structure from the obtained Lyapunov exponents, power spectra of orbital elements and distributions of induction periods based on the stagnant motion model. What we have found are the followings:

1. The global and local Lyapunov exponents show that the system is almost non-chaotic until the first close encounter between two planets and it then turns into chaotic motions with intermittent non-chaotic periods. This suggests that the phase space consists of KAM tori surrounded by the stagnant layer and immersed in the chaotic sea. In fact, the dense bands are formed in the action-angle plot, corresponding to the quasi-regular motions. The lines composing a band are undulating with frequencies that obey a power-law and this may represent the motions around the satellite tori in the stagnant layer, which have a self-similar distribution. The phase space orbit goes from one system of KAM torus and stagnant layer to another through the chaotic sea.

2. The power spectra of the orbital eccentricities of planets can be approximated by the power law, $\propto 1/f^\nu$, in general. Such power-law spectra are known to be one of the characteristic features of the stagnant motions although the power-law index is not predicted by the theory. In our models the power-law index is $\nu \simeq 1$ for the pre-encounter phase whereas it becomes $\nu \simeq 2$ after the encounter. The spectrum in the post-encounter phase is similar to that of the Brownian motions or the random walks. On the other hand, the spectrum in the pre-encounter phase might be originated from the fractional Brownian motions.

3. The distributions of the duration of the pre-encounter phase that was referred to as the induction periods obey the power law in the long-duration part. The power-law indices are substantially different between models. It is stressed that the stagnant motion model

predicts the power law for the distribution of the induction periods as a consequence of the self-similar distribution of smaller tori in the stagnant layer around a KAM torus. The distributions are deviated from the power law in the short-duration part and has a peak in between. Connecting the peaks for various models with different initial orbital separations, we have obtained the relation similar to what Chambers et al. (1996) found. It is also shown that the duration of the pre-encounter phase has actually a considerably broad distribution.

4. For the Jupiter system, the distribution of the time from the first encounter to the ejection of a planet from the system also obeys a power law, which was not expected initially. From the analogy to the stagnant motion model, we might be able to infer the phase space structure as shown schematically in Fig. 14: Many KAM tori with its own stagnant layer and satellite tori in it are distributed self-similarly in the chaotic sea.

Although we expect the phase space structure depicted in Fig. 14 is true both of the proto-planet system and the Jupiter system, the difference between them should be also mentioned. In general, the number of KAM tori in the phase space becomes smaller and the stagnant layers around them get thinner as the perturbation to the integrable system is greater. In the system of our concern, the perturbation is the interactions among the planets and hence it is larger for more massive planets. The pre-encounter phase is an exception, though. In this phase, the planets have nearly circular orbits separated by several Hill radii. Then the strength of the interactions between the planets depends only weakly on the planetary mass thanks to the definition of the Hill radius given in Eq. (2). These facts suggest that the KAM torus corresponding to the initial regular motion and its stagnant layer are robust and similar for the proto-planet and Jupiter systems while the number of other KAM tori is smaller and their stagnant layers are thinner for the Jupiter system than for the proto-planet system. This difference in the phase space structures is supposed to be responsible for the observed difference in the orbital evolutions of the two

systems: one of the planets is ejected in short times for the Jupiter system whereas no ejection occurs at least for $\sim 10^7$ years in the proto-planet system.

The results obtained in this paper appear to be consistent with our interpretation that the dynamics of three-planet system is a stagnant motion at least in the pre-encounter phase. It is also suggested from the results for the Jupiter system that even the post-encounter phase may be described by some extension of the stagnant motion model. It is true, however, that a more direct capture of satellite tori in the phase space is certainly desirable. Although we have attempted to do this with the so-called Poincare mapping, but in vain so far. We are afraid that the degree of freedom of our system is just too large to find an appropriate two dimensional section in the 12-dimensional phase space. Maybe other approaches should be pursued in the future work. In so doing, the number of realizations should be increased and other initial settings should be tried. Not to mention, we are also interested in how the results will change as the number of planets are varied.

Acknowledgments

We would like to thank Shigeru Ida and Tetsuro Konishi for their useful comments. This work was partially supported by Grants-in-Aid for the Scientific Research from the Ministry of Education, Science and Culture of Japan (17540267, 19104006) and the 21st-Century COE Program “Holistic Research and Education Center for Physics of Self-organization Systems.”

REFERENCES

- Aizawa, Y., Kikuchi, Y., Harayama, T., Yamamoto, K., Ota, M., & Tanaka, K. 1989, Prog.Theor.Phys.Suppl, 98, 36.
- Arnol'd, V. I. 1963, Uspekhi Mat. Nauk, 18(5), 13 (English transl. Russian Math. Surv., 18[5], 9)
- Baouer, W., & Bertsch, G.F. 1990, Phys.Rev.Lett. 65, 2213.
- Butler, R. P., Wright, J. T., Marcy, G. W., Fischer, D. A., Vogt, S. S., Tinney, C. G., Jones, H. R. A., Carter, B. D., Johnson, J. A., McCarthy, C., Penny, A. J. 2006, ApJ, 646, 505.
- Chambers, J. E. 2000, MNRAS, 304, 793-799
- Chambers, J. E., Wetherill, G. W. 1998, Icarus, 136, 304.
- Chambers, J. E., Wetherill, G. W. & Boss A. P., 1996, Icarus, 119, 261.
- Cincotta, P., & Simó, C. 2000, A& AS, 147, 205
- Ford, E. B. & Rasio, F. A. 2008, ApJ, 686, 621
- Gladman, B. 1993, Icarus, 106, 247
- Hirooka, H., & Saito, N. 1969, J. Phys. Soc. Japan, 26, 624
- Juric, M., & Tremaine, S. 2008, ApJ, 686, 603
- Kokubo, E., & Ida, S. 1995, Icarus, 114, 247
- Kokubo, E., Kominami, J. & Ida, S. 2006, ApJ, 642, 1131

- Kolmogorov, A. N. 1954, Dokl. Akad. Nauk SSSR, 98, 527 (English transl. in Lecture Notes in Physics, 93, Stochastic Behavior in Classical and Quantum Hamiltonian Systems, ed. G. Casati & J. Ford [Berlin: Springer], 51 [1979])
- Leichl, L. E. 1980, A Modern Course in Statistical Physics (University of Texas, Austin).
- Mandelbrot, B. B., Van Ness, W. J. 1968, SIAM.Rev., 10, 422
- Marchal, C., & Bozis, G. 1982, Celest. Mech., 26, 311
- Marzari, F., & Weidenschilling. S. J. 2002, Icarus, 156, 570.
- Moser, J. 1958, Commun. Pure Appl. Math., 11, 81
- Saito, N., Ooyama, N., Aizawa, Y., & Hirooka, H. 1970, Prog.Theor.Phys.Suppl, 45, 209.
- Shen, Y., & Turner, E., 2008, ApJ, 685, 553
- Wolf, A., Swift, J. B., Swinney, H. L., & Vastano, A. 1985, Physica D, 16, 285
- Yoshinaga, K., Kokubo, E. & Makino, J. 1999, Icarus, 139, 328
- Zhou, J.-L., Lin, D. N. C. & Sun, Y.-S. 2007, ApJ, 666, 423

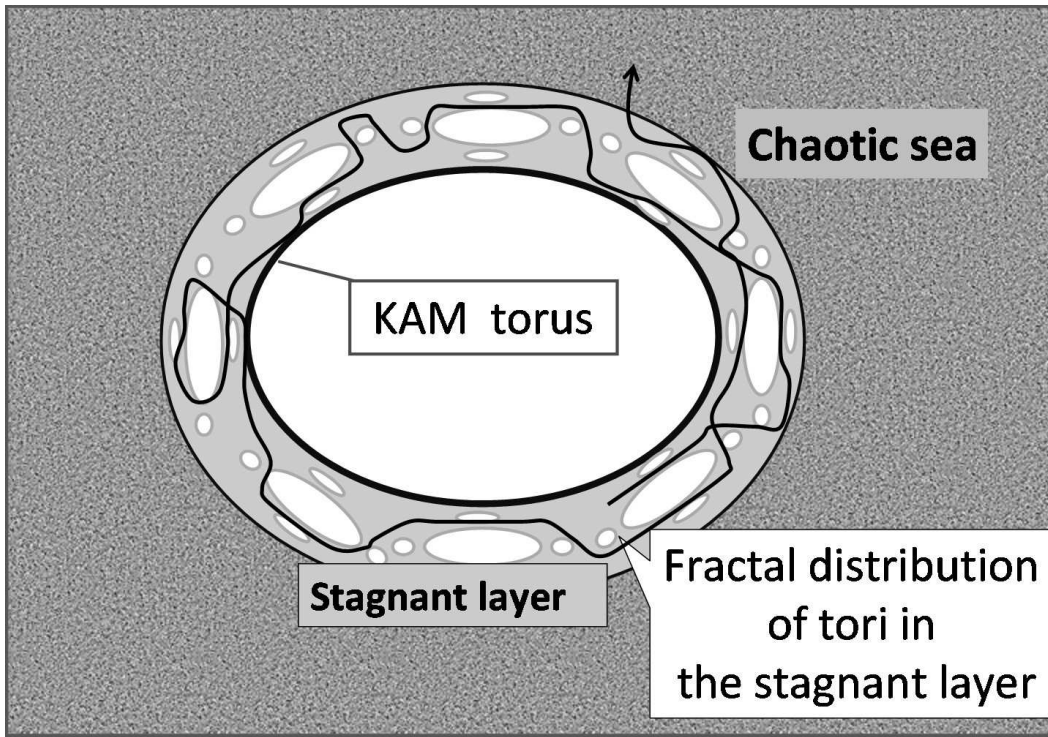


Fig. 1.— A schematic illustration of the structure in the phase space proposed by the stagnant motion model. The KAM torus is surrounded by many smaller tori distributed in a self-similar manner in the stagnant layer. An exemplary evolution in the phase space is shown by a curve with an arrow. The system is trapped by the tori in the stagnant layer and stay there for a long time, showing quasi-regular motions, which are turned into chaotic motions when the phase-space orbit escapes out of the stagnant layer into the chaotic sea.

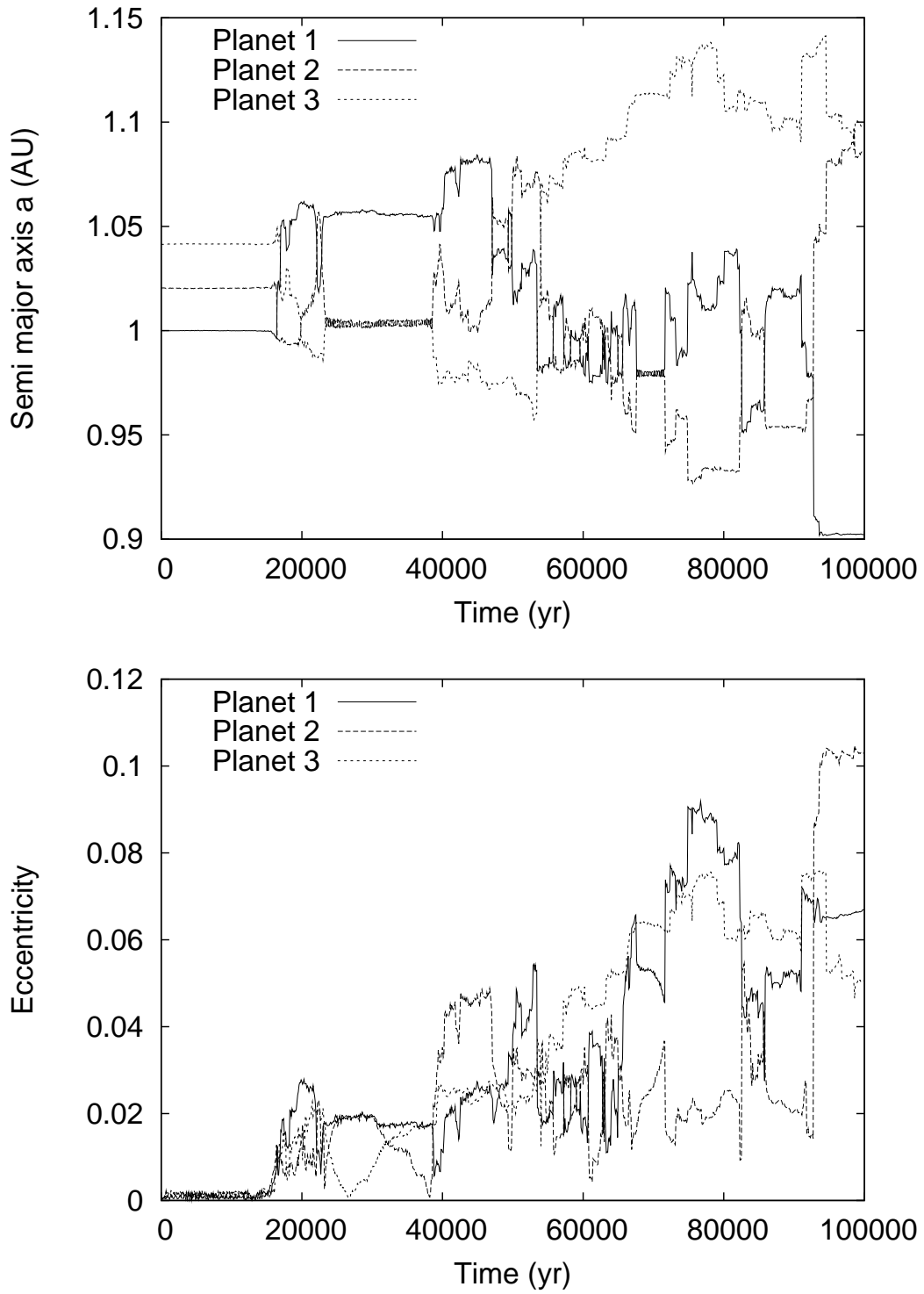


Fig. 2.— Time evolutions of the orbital semi-major axis (upper panel) and eccentricity (lower panel) of each planet for model 11.

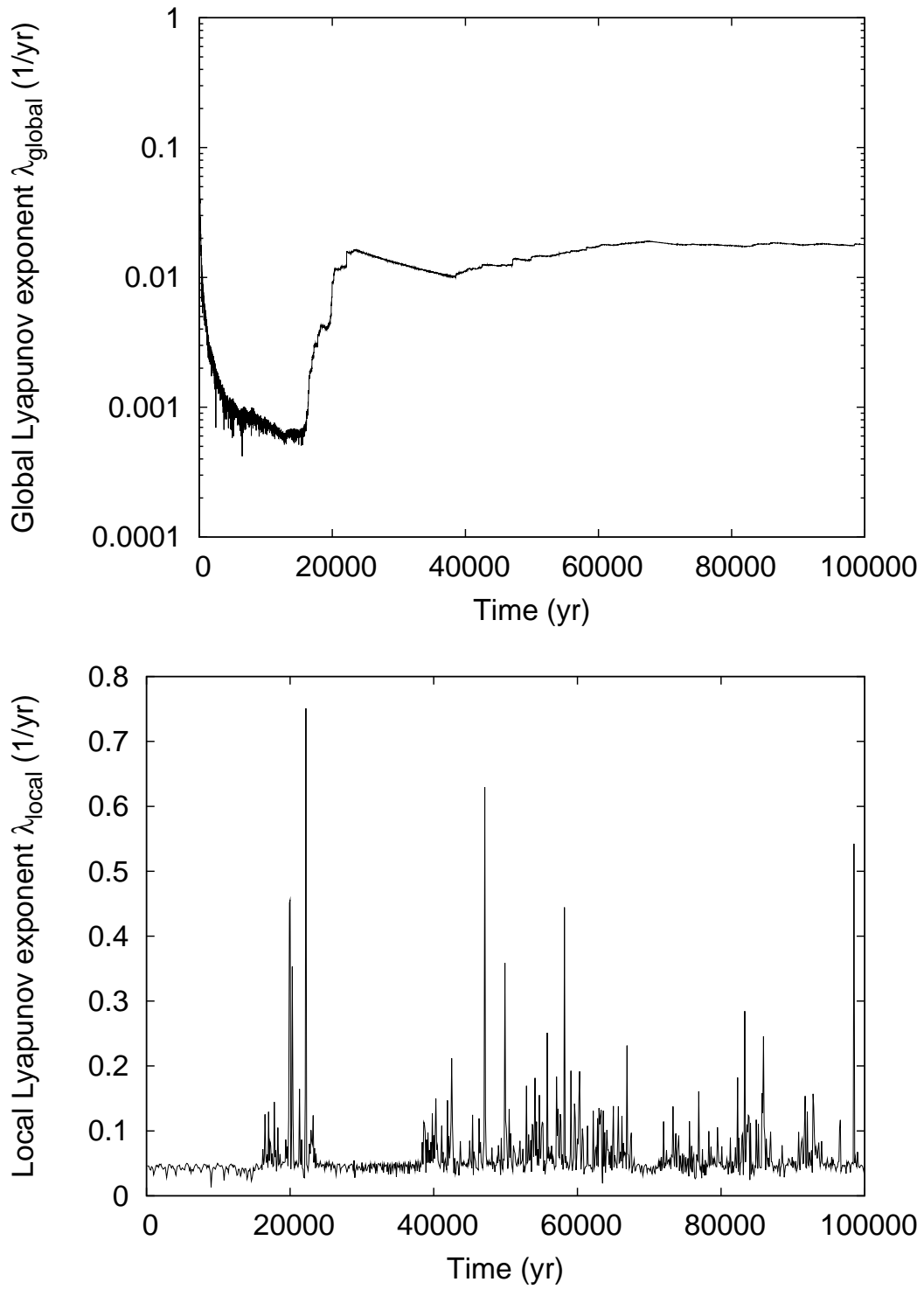


Fig. 3.— Time evolutions of the global (upper panel) and Local (lower panel) Lyapunov exponents for the same model as in Fig. 2. See the text for their definitions.

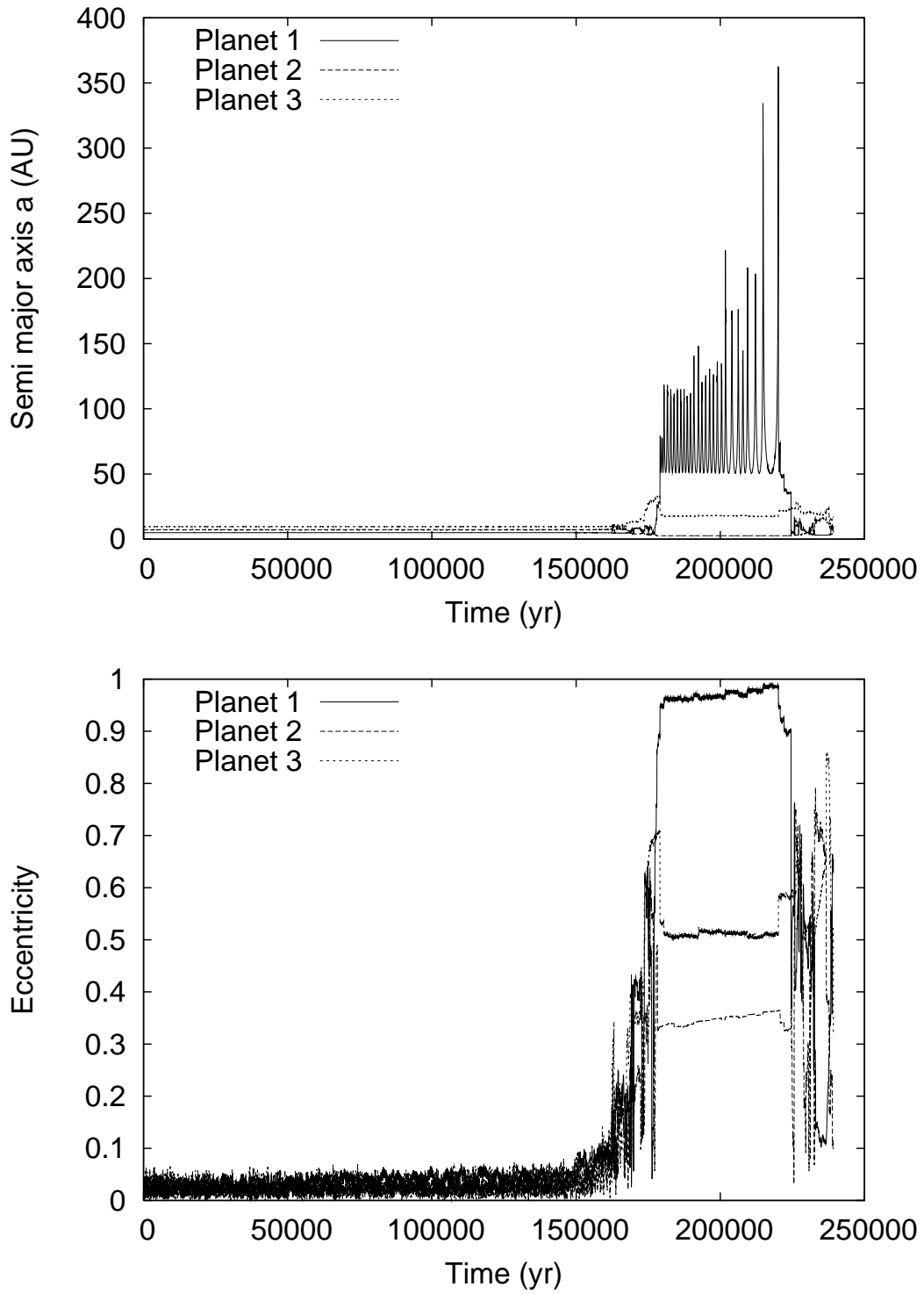


Fig. 4.— Time evolutions of the semi-major axis (upper panel) and eccentricity (lower panel) of each planet for model 17.

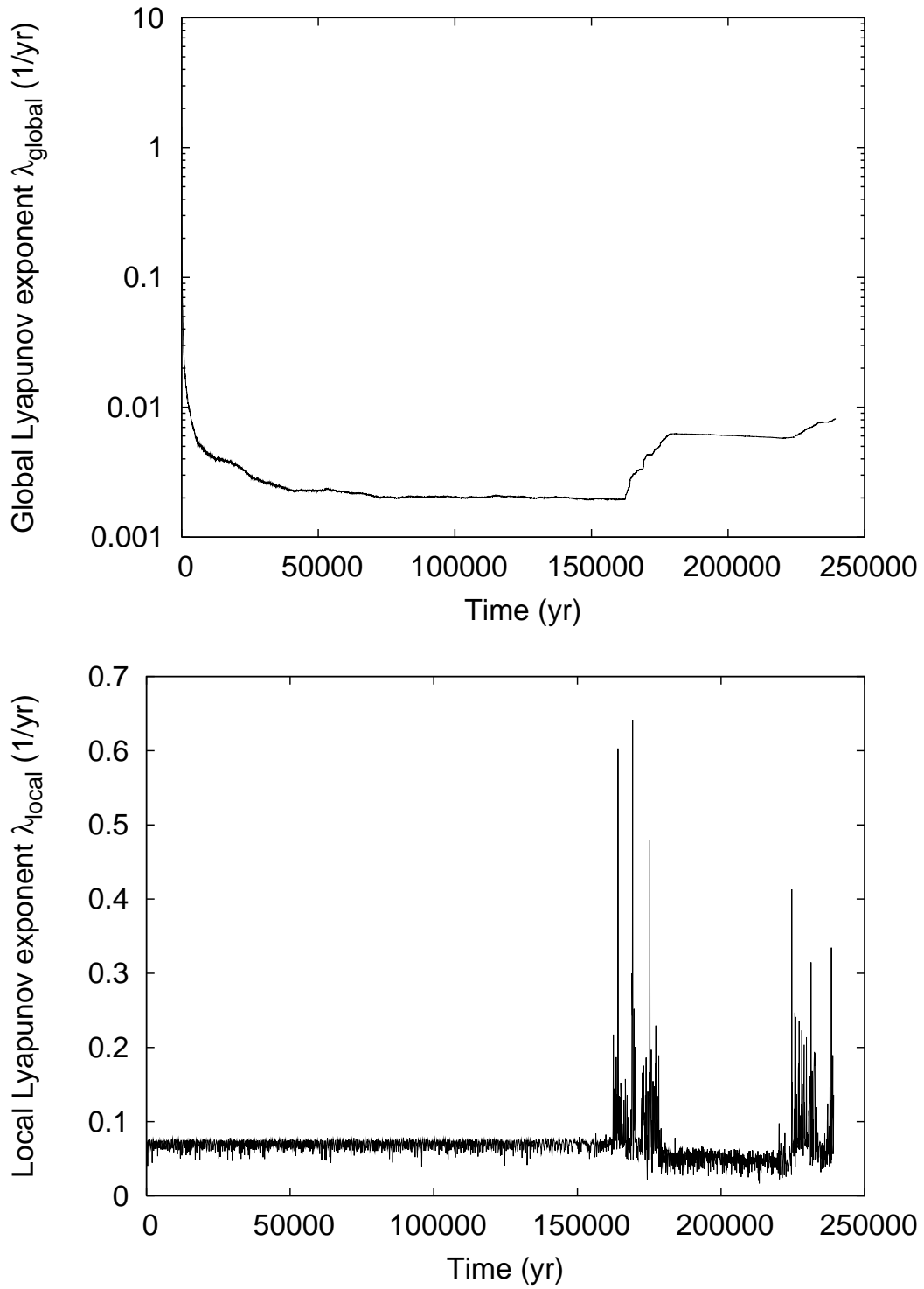


Fig. 5.— Time evolutions of the global (upper panel) and local (lower panel) Lyapunov exponents for the same model as in Fig. 4.

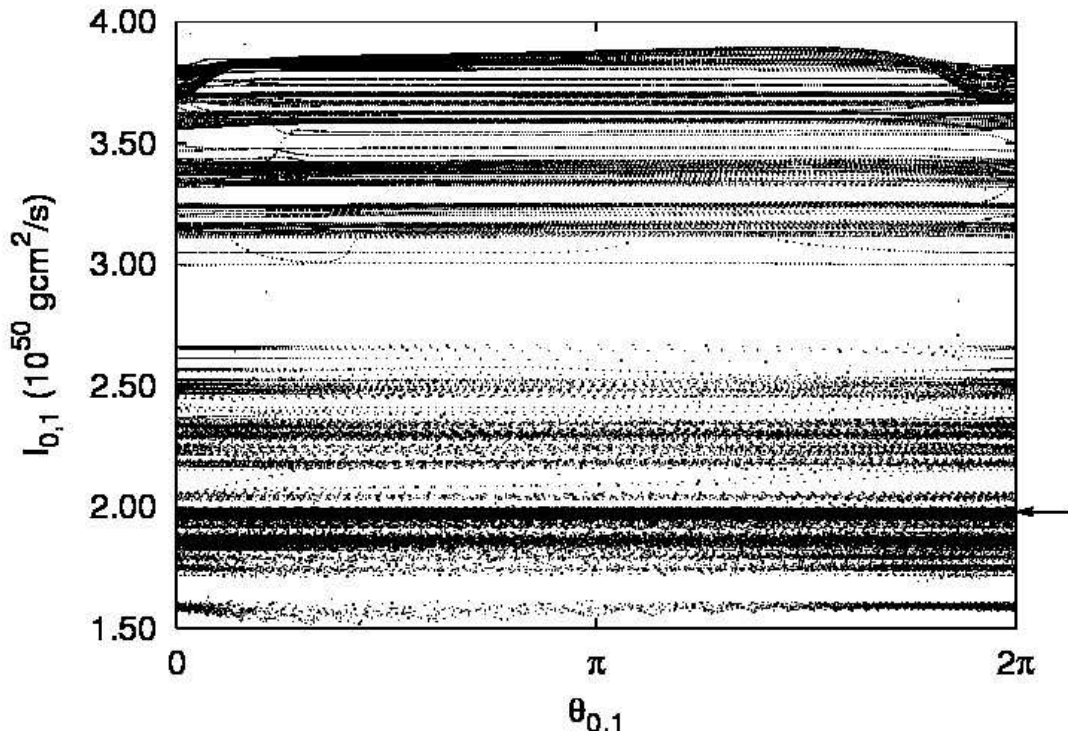


Fig. 6.— The action ($I_{0,1}$) and angle ($\theta_{0,1}$) variables for the same model as in Fig. 4. See Eq. (13) for the definitions of these variables. The horizontal line indicated by an arrow corresponds to the initial regular motion.

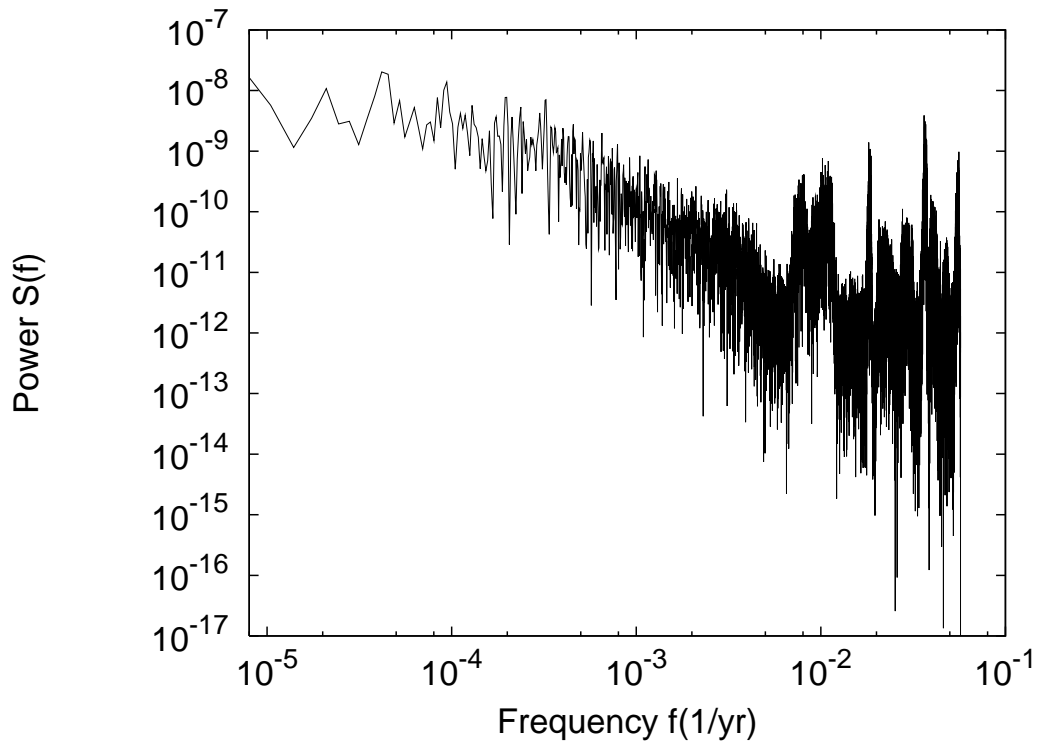


Fig. 7.— The power spectrum of the action variable ($I_{0,1}(t)$) before the close encounter for the same model as in Fig. 4 .

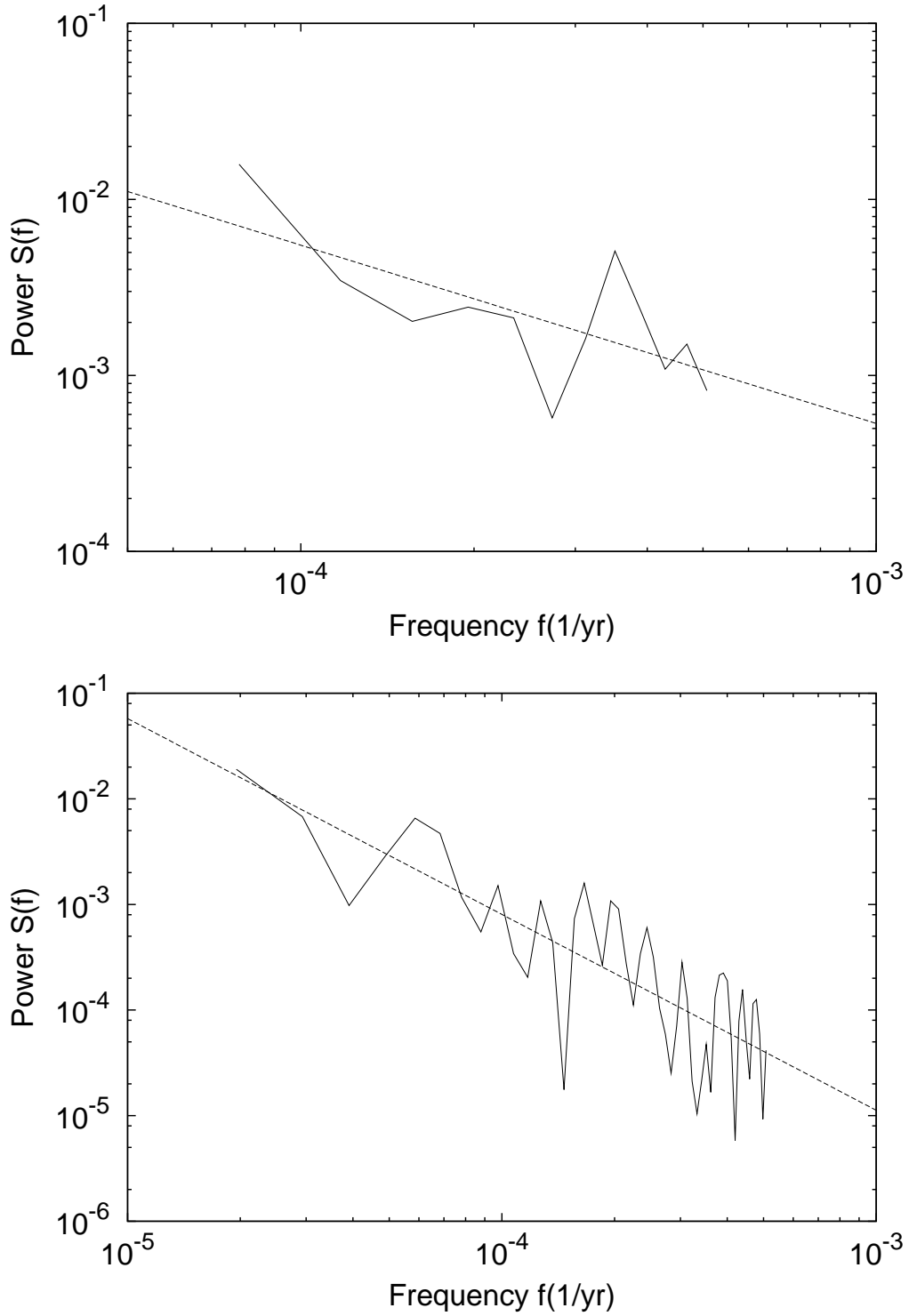


Fig. 8.— Power spectra $S(f)$ of the orbital eccentricity of the innermost planet before (upper panel) and after (lower panel) the close encounter for model 11. The straight lines are the fit to the data. The power-law indices are 1.01 and 1.85 before and after the encounter, respectively.

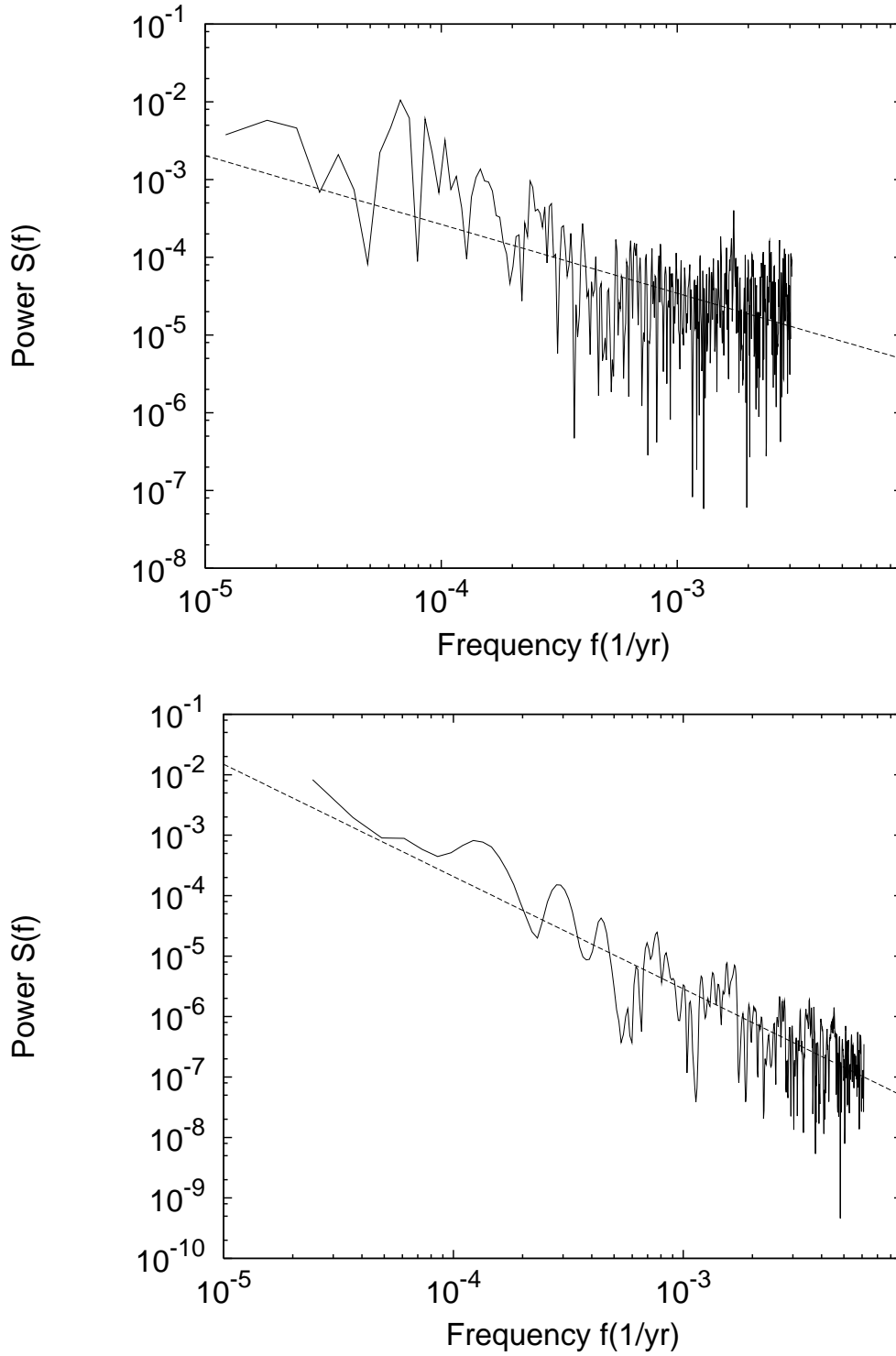
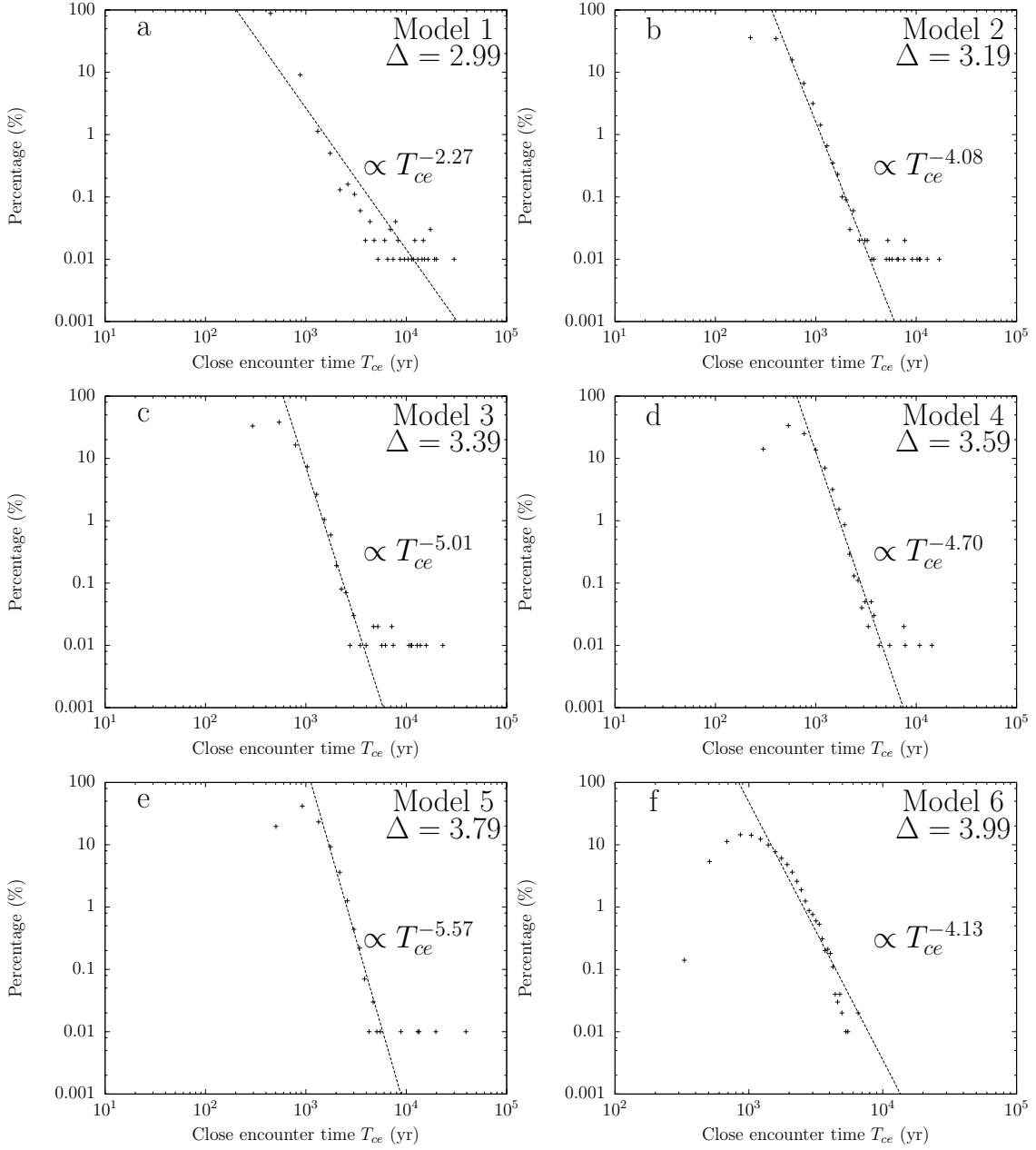
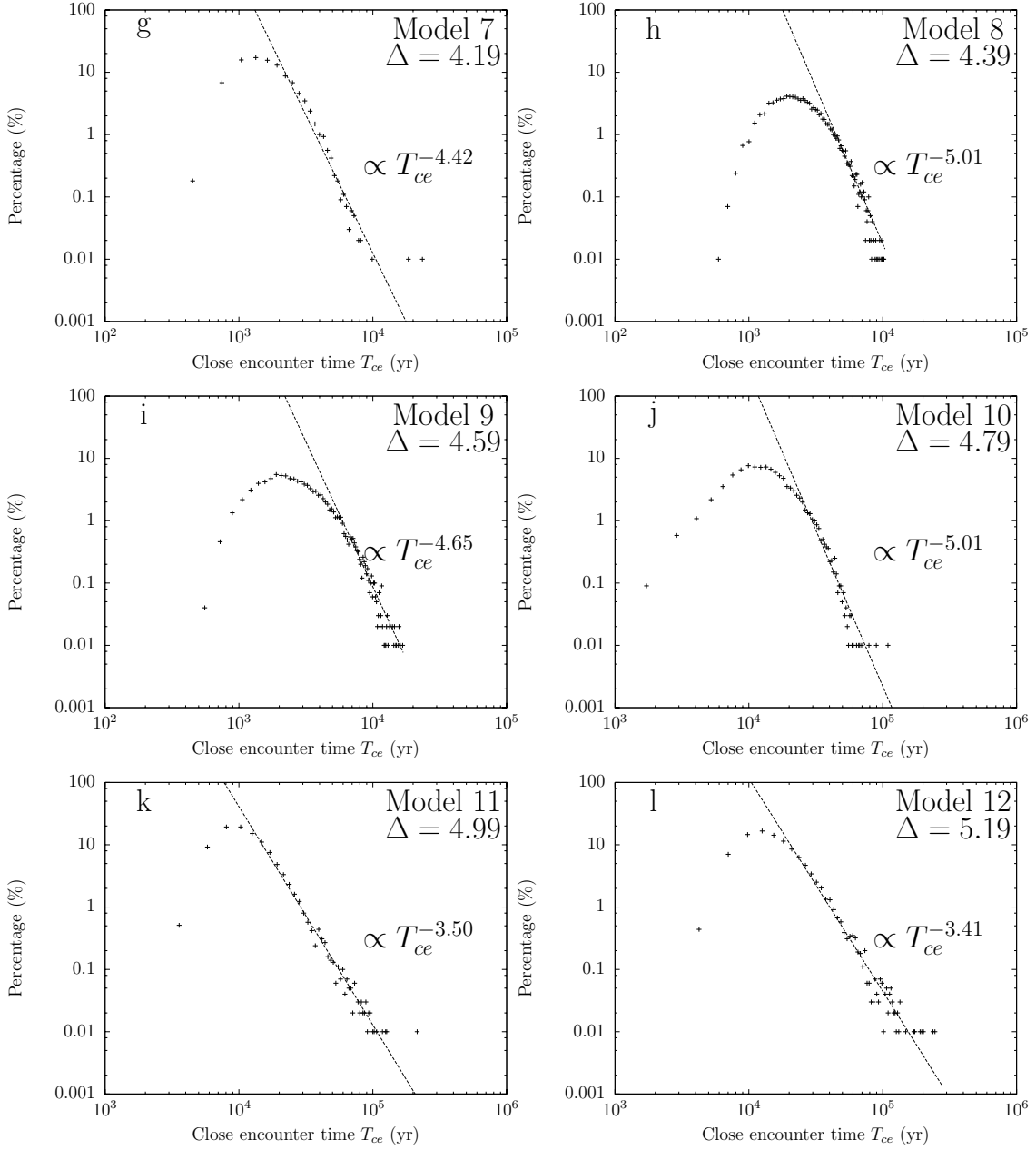


Fig. 9.— Power spectra $S(f)$ of the orbital eccentricity of the innermost planet before (upper panel) and after (lower panel) the close encounter for model 17. The straight lines are the fit to the data. The power-law indices are 0.88 and 1.85 before and after the encounter, respectively.





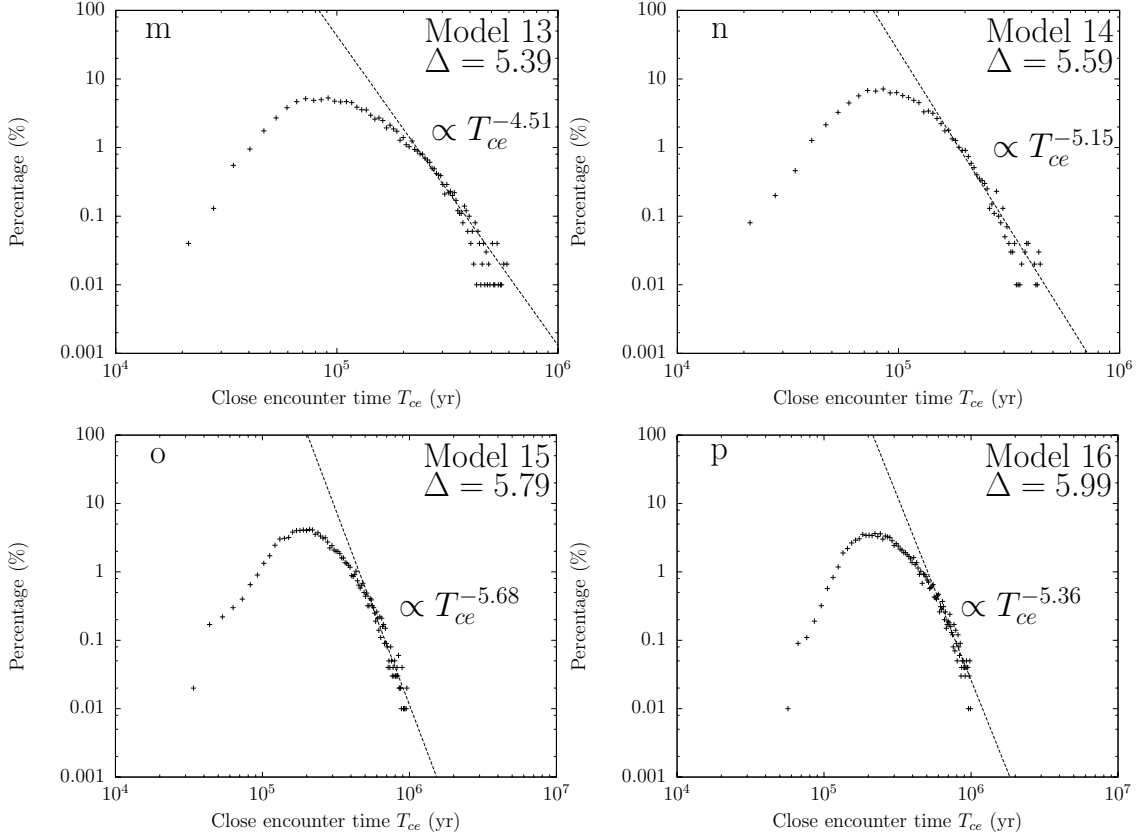


Fig. 10.— Normalized distributions of the duration of the pre-encounter phase, T_{ce} , for models 1 to 16. The straight lines are the fit by power law to the data in the long-duration regime.

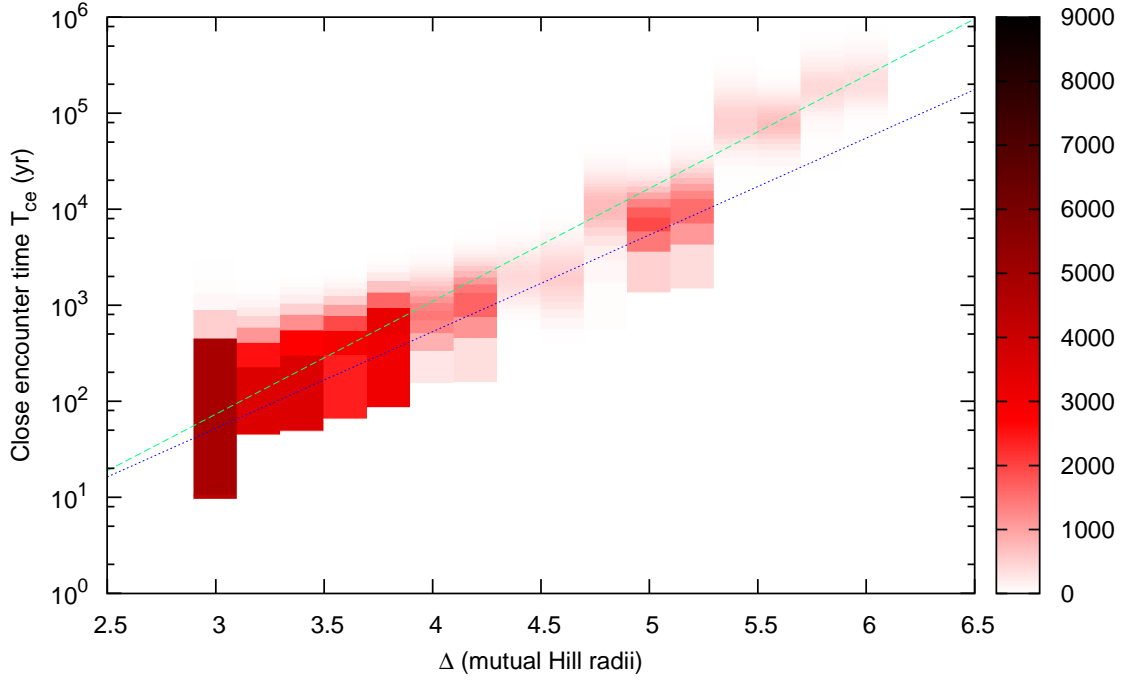


Fig. 11.— Histogram for models 1 through 16 in the plane of the initial orbital separation Δ and the duration of the pre-encounter phase, T_{ce} . The number of cases is expressed in color. The blue dotted line is the fit to the peak (Eq. (16)) and the green dashed line shows the $\Delta - T_{ce}$ relation in Chambers et al. (1996).

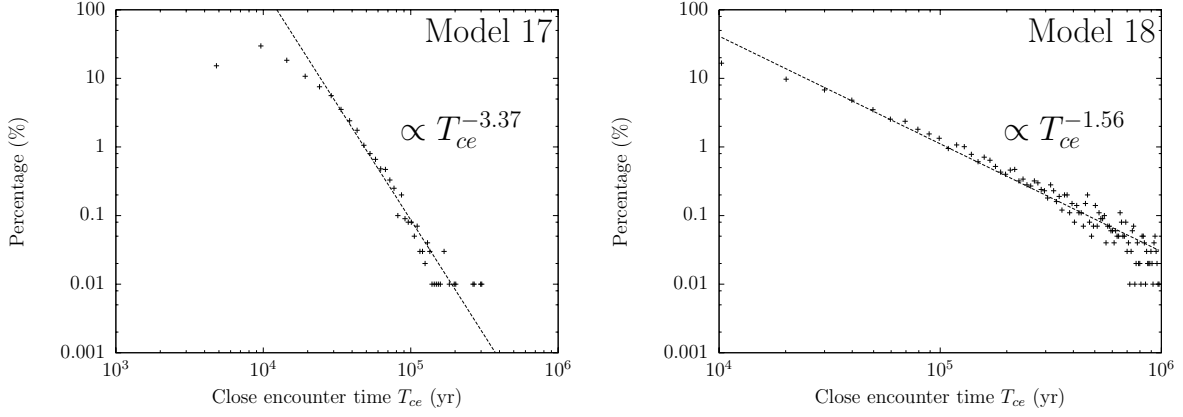


Fig. 12.— Normalized distributions of the duration of the pre-encounter phase, T_{ce} , for models 17 (left panel) and 18 (right panel). The straight lines are the fit by power law to the data in the long-duration regime.

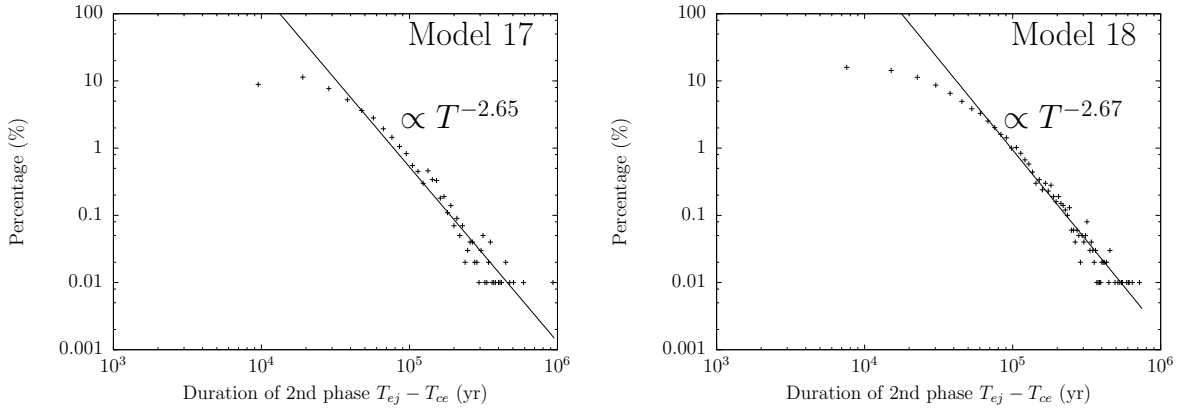


Fig. 13.— Normalized distributions of the time from the first close encounter up to the ejection of a planet, $T_{ej} - T_{ce}$, for models 17 (left panel) and 18 (right panel). The straight lines are the fit by power law to the data in the long-time regime.

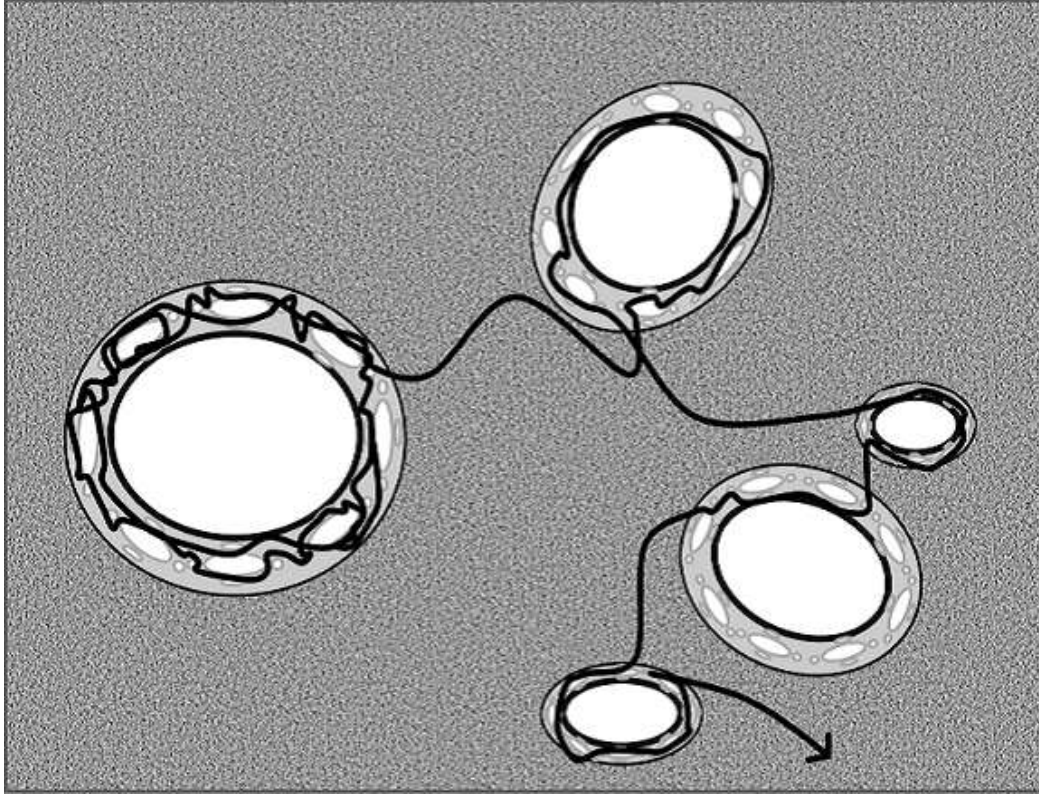


Fig. 14.— A schematic illustration of the phase space suggested by the power-law distributions of the time from the encounter to the ejection of a planet for the Jupiter system. KAM tori of various sizes with a stagnant layer and smaller tori in it are distributed self-similarly in the chaotic sea. An exemplary phase space orbit is given by a curve with an arrow.

Table 1. Model parameters

Model	m_{pl} (M_{\odot})	a_1 (AU)	E_{tot} ($\times 10^{39}$ erg)	L_{ztot} ($\times 10^{46}$ gcm ² s ⁻¹)	P_{xtot} ($\times 10^{30}$ cms ⁻¹)	P_{ytot} ($\times 10^{30}$ cms ⁻¹)	$\langle \Delta \rangle$ (σ_{Δ}^2) (Hill radius) ^a $\langle a_2 \rangle$ ($\sigma_{a_2}^2$), $\langle a_3 \rangle$ ($\sigma_{a_3}^2$) (AU)	$\langle e \rangle$ (σ_e^2)
1	10^{-7}	1	-2.6152	2.6752	-3.0924	5.3780	2.9970 (1.3965 $\times 10^{-4}$)	1.2129×10^{-7} (3.7549 $\times 10^{-15}$)
2	10^{-7}	1	-2.6131	2.6763	-3.2966	5.7347	3.1973 (1.1031 $\times 10^{-4}$)	1.2123×10^{-7} (3.7505 $\times 10^{-15}$)
3	10^{-7}	1	-2.6110	2.6774	-3.5005	6.0910	3.3975 (8.9031 $\times 10^{-5}$)	1.2118×10^{-7} (3.7451 $\times 10^{-15}$)
4	10^{-7}	1	-2.6089	2.6785	-3.7042	6.4472	3.5977 (7.3037 $\times 10^{-5}$)	1.2112×10^{-7} (3.7404 $\times 10^{-15}$)
5	10^{-7}	1	-2.6068	2.6796	-3.9076	6.8031	3.7979 (6.0711 $\times 10^{-5}$)	1.2105×10^{-7} (3.7370 $\times 10^{-15}$)
6	10^{-7}	1	-2.6047	2.6806	-4.1108	7.1587	3.9980 (5.1030 $\times 10^{-5}$)	1.2100×10^{-7} (3.7317 $\times 10^{-15}$)
7	10^{-7}	1	-2.6026	2.6817	-4.3137	7.5142	4.1982 (4.3308 $\times 10^{-5}$)	1.2094×10^{-7} (3.7274 $\times 10^{-15}$)
8	10^{-7}	1	-2.6005	2.6828	-4.5164	7.8693	4.3983 (3.7065 $\times 10^{-5}$)	1.2088×10^{-7} (3.7223 $\times 10^{-15}$)
9	10^{-7}	1	-2.5985	2.6839	-4.7188	8.2243	4.5984 (3.1962 $\times 10^{-5}$)	1.2082×10^{-7} (3.7183 $\times 10^{-15}$)
10	10^{-7}	1	-2.5964	2.6850	-4.9210	8.5790	4.7985 (2.7747 $\times 10^{-5}$)	1.2076×10^{-7} (3.7138 $\times 10^{-15}$)
11	10^{-7}	1	-2.5943	2.6861	-5.1229	8.9335	4.9986 (2.4236 $\times 10^{-5}$)	1.2070×10^{-7} (3.7094 $\times 10^{-15}$)
12	10^{-7}	1	-2.5922	2.6872	-5.3246	9.2877	5.1986 (2.1286 $\times 10^{-5}$)	1.2064×10^{-7} (3.7047 $\times 10^{-15}$)
13	10^{-7}	1	-2.5902	2.6883	-5.5261	9.6417	5.3987 (1.8791 $\times 10^{-5}$)	1.2058×10^{-7} (3.7013 $\times 10^{-15}$)
14	10^{-7}	1	-2.5881	2.6894	-5.7273	9.9955	5.5988 (1.6665 $\times 10^{-5}$)	1.2052×10^{-7} (3.6969 $\times 10^{-15}$)
15	10^{-7}	1	-2.5860	2.6905	-5.9282	10.349	5.7988 (1.4844 $\times 10^{-5}$)	1.2047×10^{-7} (3.6916 $\times 10^{-15}$)
16	10^{-7}	1	-2.5840	2.6916	-6.1290	10.702	5.9989 (1.3274 $\times 10^{-5}$)	1.2040×10^{-7} (3.6874 $\times 10^{-15}$)
17	10^{-3}	5	-4.0528×10^3	6.9568×10^4	-2.7455×10^5	5.2670×10^5	3.3968 (3.3889 $\times 10^{-4}$)	1.0252×10^{-3} (2.4813 $\times 10^{-7}$)
18	10^{-3}	5	-3.9198×10^3	7.1002×10^4	-2.4088×10^5	5.8830×10^5	^a $\langle a_2 \rangle = 7.2509$ (8.5876 $\times 10^{-4}$) , $\langle a_3 \rangle = 9.4989$ (1.1202 $\times 10^{-3}$)	1.0138×10^{-3} (2.4088 $\times 10^{-7}$)

Note. — a_1 : the semi-major axis of the innermost planet. E_{tot} : the total energy. L_{ztot} : the z-component of the total angular momentum. P_{xtot}, P_{ytot} : the x- and y-components of the total linear momentum. $\langle \Delta \rangle, \sigma_{\Delta}^2$: the mean and variance of the planetary orbital separations over 10000 realizations. $\langle e \rangle, \sigma_e^2$: the mean and variance of the planetary eccentricity over 10000 realizations. For each realization the mean eccentricity over three planets, e , is obtained and then $\langle e \rangle$ and σ_e^2 are computed.

^a $\langle a_2 \rangle, \sigma_{a_2}^2, \langle a_3 \rangle, \sigma_{a_3}^2$: the mean and variance of the semi-major axis of the second and third planets.

Table 2. The Power Spectral Index for the Proto-Planet Systems

Model	Orbital separation Δ (Hill radius)	power-law index ν					
		sample 1		sample 2		sample 3	
		1st phase	2nd phase	1st phase	2nd phase	1st phase	2nd phase
1	2.9970	-	2.12	-	1.85	-	1.95
2	3.1973	-	1.59	-	2.06	-	1.36
3	3.3975	-	1.61	-	2.38	-	1.79
4	3.5977	-	1.83	-	1.59	-	2.03
5	3.7979	-	2.00	-	1.70	-	1.43
6	3.9980	-	2.03	-	1.52	-	1.90
7	4.1982	-	1.91	-	2.00	-	1.73
8	4.3983	-	1.66	-	2.01	-	1.79
9	4.5984	-	1.67	-	1.66	-	2.08
10	4.7985	0.10	1.89	0.65	2.01	1.27	1.39
11	4.9986	-	2.12	1.01	1.85	-	1.95
12	5.1986	0.75	1.62	-	1.92	0.91	2.31
13	5.3987	0.83	0.93	0.93	1.90	0.68	1.96
14	5.5988	0.84	1.85	1.25	1.97	0.85	1.96
15	5.7988	0.92	1.88	0.92	1.93	0.50	1.86
16	5.9989	1.09	1.80	0.65	1.84	0.90	1.95

Note. — The power spectra of the orbital eccentricity for the innermost planet are fit by the power law. Three realizations are arbitrarily chosen among 10000 realizations for each model and shown as samples 1, 2 and 3. The pre- and post-encounter phases are treated separately and referred to as 1st and 2nd phases in the table, respectively. For some of the models, the duration of the phase is too short to obtain the power-law index and "-" is put instead of the index. The averages of ν over all the models in this table are 0.84 before the encounter and 1.84 after the encounter.

Table 3. The Power Spectral Index for the Jupiter Systems

Model	Orbital separation	power-law index ν					
		sample 1		sample 2		sample 3	
		1st phase	2nd phase	1st phase	2nd phase	1st phase	2nd phase
1	$\langle \Delta \rangle = 3.3968$ (Hill radius)	0.88	1.85	1.69	1.55	0.00	1.72
2	$\langle a_2 \rangle = 7.2509, \langle a_3 \rangle = 9.4989$ (AU)	0.99	1.87	1.03	1.78	0.99	1.87

Note. — The power spectra of the orbital eccentricity for the innermost planet are fit by the power law. The averages of ν over the models in the table are 0.91 before the encounter and 1.77 after the encounter.